# DEVELOPMENT OF CONTROL STRATEGY FOR POWER MANAGEMENT IN HYBRID RENEWABLE ENERGY SYSTEM

**Lalita Jhala, Raunak Jangid, Kapil Parikh**
**E-Mail id: raunak.ee85@gmail.com**
**Department of Electrical Engineering, SITE Nathdwara, Rajasthan, India**

**Abstract-** This paper presents the power management and control strategy of a hybrid wind- solar PV system. The developed control strategy is implemented of the proposed hybrid system entails two main buses i.e., an AC and a DC. Wind and solar PV array systems rated capacity are 8.5kW and 10kW respectively. Both are connected to DC bus via their associated converters and MPPT controller derived optimal torque (OT). The hybrid system also has incorporated battery with DC bus via DC-DC converter. The inverter provides the interfacing between both the buses which is based fuzzy system& multilevel inverter. The load connected receives three phase AC supply from AC bus. The battery does the role of Energy storage system (ESS) in the event of excess power. While the rise in demand it also acts as a standby unit. The system elaborated here always tends to keep battery's state of charge (SOC) above 80%. Hence, manages power. Performance of the ESS has been shown via the results obtained from MATALAB/Simulink under several operation modes.
**Keywords:** PV Array, Wind Turbine, Battery, Power management unit (PMU).

## 1. INTRODUCTION

The Renewable energy sources (RES) have now been relied upon more regularly. It has provided us the other option for clean energy generation compared to conventional sources. PV systems and wind systems can easily be taken as the alternate source of generation for the like of area remotely located. With combination of both is system i.e. to have hybrid system further decreases standalone power supply growth cost. Nonetheless, it's a reliable option for power supply [1]-[2]. A power system is said to be hybrid when it comprises of fossil powered generator along with RES [3]. But the RES like wind and solar PV array has some disadvantages too. These are dependent on the surrounding environment as in case of wind system its output changes as the speed of wind changes. Same is true for PV array as it varies as the solar isolation. Hence, the output of these RES is different for different day and month of the year. Also, the RES hybrid system is not grid connected and hence suitable for the remote location installation as this kind of location doesn't have access to grid. Since cost of fuel and infrastructure increases for the extension of grid to very remote areas. To make it a more reliable system these are associated with battery for all the working conditions [4]. Using a RES hybrid system that has the facility of storage of energy can easily keep out diesel powered generator. For hybrid system discussed here there are several topologies [5]. This includes the conditioning of power and ESS also it emphasizes on optimal control for maximum transfer of energy. Presented work aims to the idea of hybrid system configuration, dynamic modeling, power management, and control strategies. The author proposes and investigates control strategy for standalone hybrid solar-wind system power management for different operating conditions. Due to the uninterrupted demand for energy, batteries backups are used in the hybrid system. So, the suggested system is efficient for working under variable and load conditions.

## 2. HRES CONFIGURATION & MODELING

Fig. 2.1shows the developed control strategy for energy management is implemented on stand-alone hybrid wind-solar PV system. For efficient power management between WES, solar PV and battery storage system (BSS), power management unit (PMU) is proposed. The main objective of this unit is to control the power flow between the dc bus and different sources.
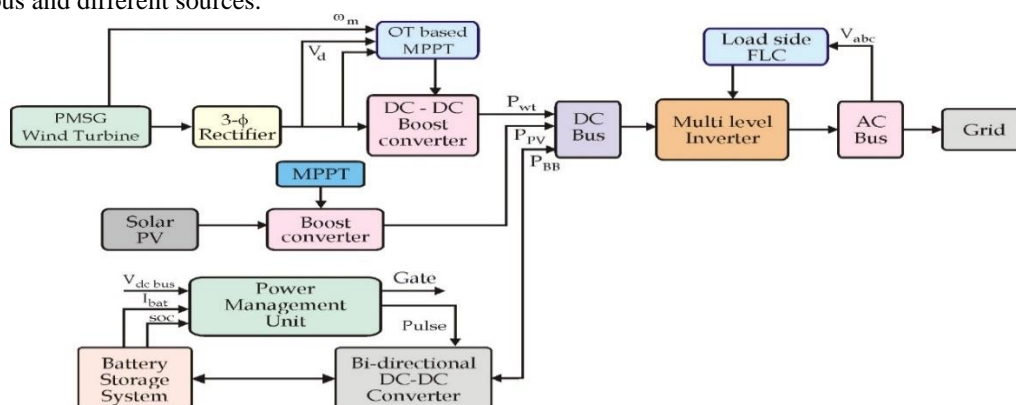


**Fig. 2.1 Block Diagram of Power Management Unit (PMU) for Stand-Alone HRES**

## 3. PV SYSTEM MODELING

PV cell's equivalent circuit is given in Fig. 3.1 .$I_{ph}$=Cell/Module photocurrent(A). $R_{sh}$ = intrinsic shunt of cell& $R_s$= cell series resistances of cell. $R_{sh}$ has a huge value where as $R_s$ is very small. Therefore, for the purpose of analysis both can be neglected. The generation of electrical power takes place in PV system by PV arrays. These PV arrays are arrangement of it single unit modules in either series or parallel. One module unit of PV is created by grouping several PV cells. In Fig. 3 PV array's equivalent circuit is outlined.

The expression for solar cell characteristics for voltage-current relations is,

$$I_{ph} = [I_{SC} + K_i (T - 298)] * I_r /1000$$

$I_{sc}$=current in short circuit condition(A), $K_i$=cell's $I_{sc}$ at 25°C & 1000W/m², T=operating temperature(K), $I_r$=solar irradiation(W/m²).

Expression for reverse saturation current($I_{rs}$) of PV module,

$$I_{rs} = I_{sc} /[\exp (qV_{oc} /N_S knT) - 1]$$

q=electron charge=$1.6 \times 10-19$C, $V_{oc}$=voltage in open circuit condition(V), Ns=cells connected no. in series, n=diode ideality factor, k=Boltzmann's constant= $1.3805 \times 10-23$J/K.
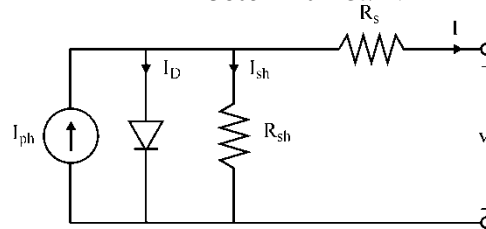


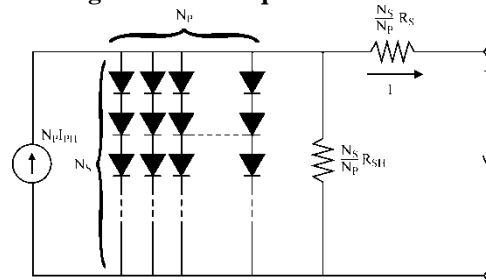**Fig. 3.1 PV cell equivalent circuit**



**Fig. 3.2 Solar arrays equivalent circuit**

Expression for module saturation current($I_0$) is given below and it changes with cell temperature,

$$I_0 = I_{rs} \left[\frac{T}{T_r}\right]^3 \exp \left[\frac{q \times E_{g0}}{nk}\left(\frac{1}{T} - \frac{1}{T_r}\right)\right] \quad (1)$$

$T_r$=nominal temperature=298.15K, $E_{g0}$=semiconductor's band gap energy=1.1eV.PV module output current,

$$I = N_P \times I_{ph} - N_P \times I_0 \times \left[\exp \left(\frac{V/N_S + I \times R_S/N_P}{n \times V_t}\right) - 1\right] - I_{sh} \quad (2)$$

With $V_t = \frac{k \times T}{q}$ and $I_{sh} = \frac{V \times N_P/N_S + I \times R_S}{R_{sh}}$

Np=PV modules connected no.in parallel, $V_t$=diode thermal voltage(V).

**Table 3.1 Electrical characteristics data of Sun Power Module**

| Parameter | Value |
|---|---|
| Rated value of power($W_{mp}$) | 305.226 W |
| Voltage value when power has maximum value($V_{mp}$) | 54.7 V |
| Current value when power has maximum value($I_{mp}$) | 5.58 A |
| Voltage when Open circuit($V_{OC}$) | 64.2 V |
| Current in Short circuit condition($I_{SC}$) | 5.96 A |
| Total Series-connected modules per string | 11 |
| Total Parallel strings | 3 |
| System's Maximum value of voltage | 700 V |
| Operating temperature range | −40 °C to 80 °C |

## 4. WIND SYSTEM MODELING

It can be seen from the block diagram optimal torque with MPPT method shown in Fig.4.1 MPPT tool execute a torque reference accomplished of extracting maximum power at any wind speed. The curve $T_{opt}$ is expressed by:

International Journal of Technical Research & Science

$$T_{opt} = K_{opt} * \omega_{opt}^2 \tag{1}$$

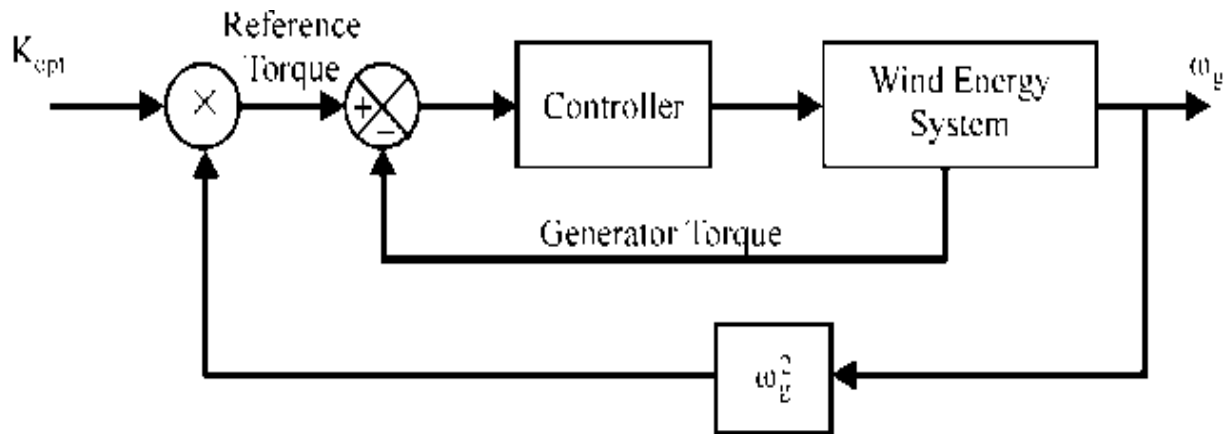$$K_{opt} = 0.5 * \rho\, A * \left(\frac{r_m}{\lambda_{opt}}\right)^3 * C_{P-max} \tag{2}$$



**Fig. 4.1 Optimal torque control with MPPT method**

PMSG currents are:

$$\frac{di_{md}}{dt} = \frac{1}{L_d}(v_d - R_{st}i_d + \omega L_q i_{mq}), \tag{3}$$

$$\frac{di_{mq}}{dt} = \frac{1}{L_d}(v_q - R_{st}i_q + \omega L_q i_{md} - \omega\,\psi_{PM}), \tag{4}$$

$$i_d = \frac{1}{R_c}(L_d\frac{di_{md}}{dt} - \omega L_q i_{mq} + R_c i_{md}), \tag{5}$$

$$i_q = \frac{1}{R_c}(L_q\frac{di_{mq}}{dt} + \omega L_d i_{md} + \omega\,\psi_{PM} + R_c i_{mq}), \tag{6}$$

$$i_{cd} = i_d - i_{md}, \tag{7}$$

$$i_{cq} = i_q - i_{mq}, \tag{8}$$

**Table-4.1 Parameter of wind turbine model**

| Parameter | Value |
|---|---|
| Mechanical power output at nominal rating(W) | 8.5e3 |
| Electrical generator's value of Base power(VA) | 8.5e3/0.9 |
| Wind speed's base value(m/s) | 12 |
| Maximum power when wind's speed is at base value(nominal rated mechanical power's p.u.) | 0.8 |
| Rotational speed's base value(base generator speed's p.u.) | 1 |
| wind-turbine power characteristics of Pitch angle beta to display (beta >=0)(deg) | 0 |

$i_d, i_q = d_q$ axes currents, $V'_d, V_q = d_q$ axes voltages, $i'_{cd}, i_{cq} = d_q$ axes iron losses currents, $i_{md}, i_{mq} = d_q$ axes magnetizing currents, $L_d, L_q = d_q$ axes inductances.

PMSG Electromagnetic torque equation,

$$T_e = \frac{2}{3}p\left[\psi_{PM}i_{mq} + (L_d - L_q)i_{md}i_{mq}\right] \tag{9}$$

## 5. MODELING OF BATTERIES

Fig. 5.1 displays the blocks that are used to build the battery equivalent circuit. Its parameters have been set so as to get best rechargeable battery.
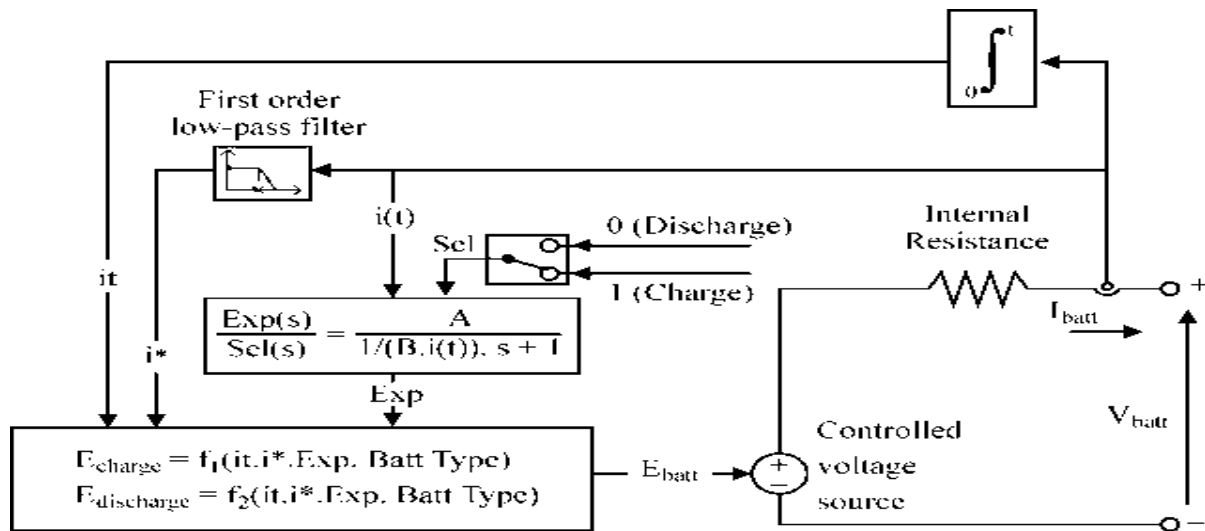
**Fig. 5.1 Battery equivalent circuit**

Mathematical modeling of battery is based on the equation written below for different types i.e. Nickel-cadmium(NiCd)&Ni-metal-hydride based,

**Discharge Model (i* > 0)** $f_1(it, i*, i, Exp) = E_0 - K \cdot \frac{Q}{Q-it} \cdot i* - K \cdot \frac{Q}{Q-it} \cdot it + \text{Laplace}^{-1}\left(\frac{Exp(s)}{Sel(s)} \cdot 0\right)$

**Charge Model (i* < 0)** $f_2(it, i*, i, Exp) = E_0 - K \cdot \frac{Q}{|it|+0.1 \cdot Q} \cdot i* - K \cdot \frac{Q}{Q-it} \cdot it + \text{Laplace}^{-1}\left(\frac{Exp(s)}{Sel(s)} \cdot \frac{1}{s}\right).$

$E_{Batt}$=nonlinear voltage(V), $E_0$=constant voltage(V), Exp(s)=exponential zone dynamics(V), Sel(s)=battery mode, when battery discharge s=0 & when it is charging s=1. K=polarization constant(Ah$^{-1}$), i*=low frequency current dynamics(A), i=battery current(A).it is extracted capacity(Ah).Q=maximum battery capacity(Ah), A=exponential voltage(V), B=exponential capacity(Ah$^{-1}$).

## 6. DESIGN OF LOAD FLC (LFLC)

The fuzzy logic controlled PWM inverter is used to supply balance power to the proposed system. The FLC inverter is coupled to the PV-wind- battery storage system and used to clamps the output voltage at desired level by using two fuzzy inputs i.e., errors (E) and change of error (COE). The "if and then rule" based fuzzy rule matrix is described in Table 3.8.In the proposed control strategy, fuzzy control generates desired gate pulse for PWM inverter. MAMDANI fuzzy interface is used to develop 49 rule bases, which are applied to PWM inverter to generates desired gate pulse. The gate pulse of desired magnitude to the IGBT based inverter is generated by a pulse generator. The FLC inverter have an ability to make balance between different energy sources of micro grid and restricts the voltage output at desired level.

The fuzzy logic controller developed for the load bus reference voltage (LFLC). Fuzzification, defuzzification, and inference engine are three main blocks of the diagram. The load fuzzy logic controller receives the error E and change of error dEas inputs. Fig. 6.1 shows the block diagram of the load fuzzy logic controller (LFLC).
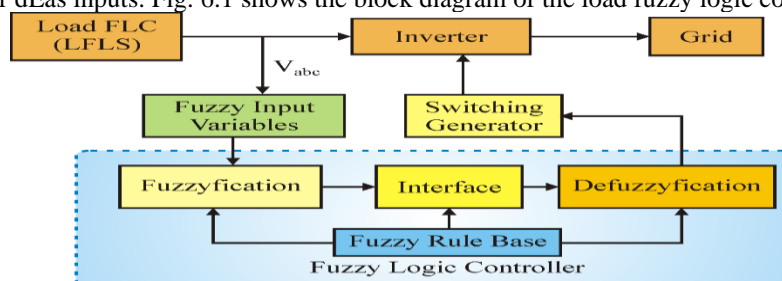


**Fig. 6.1 Block Diagram of LFLC based Controller**

### 6.1 Fuzzification

The error E and change of error CE will be calculated. The error and change in error are the inputs of the LFLC. It is given to the LFLC as inputs, which produce the duty cycle ($\alpha$) as output. This duty ratio as output is used to generate the switching pulses for the inverter, to minimize the switching loss of the inverter circuit. The seven linguistic variables are assigned to input and output variables as shown

### 6.1.1 Error (E)

It is divided into seven linguistic variables as Positive small (PS), Positive Medium (PM) and Positive Large (PL), Negative Large (NL), Negative medium (NM), Negative small (NS), Zero error (ZE). It lies within the range of [-1 1].

### 6.1.2 Change in Error (dE)

It is classified into seven linguistic variables as Negative Large (NL), Negative medium (NM), Negative small

(NS), Zero error(ZE), positive small(PS), positive Medium(PM) and positive Large(PL). It lies within the range of [-1 1].

### 6.1.3 Duty Ratio α (Output-1)

It is classified into seven linguistic variables as Negative Large (NL), Negative Medium(NM), Negative Small(NS), Zero Error(ZE), Positive Small(PS), Positive Medium(PM) and Positive Large(PL). It lies within the range of [-1 1].
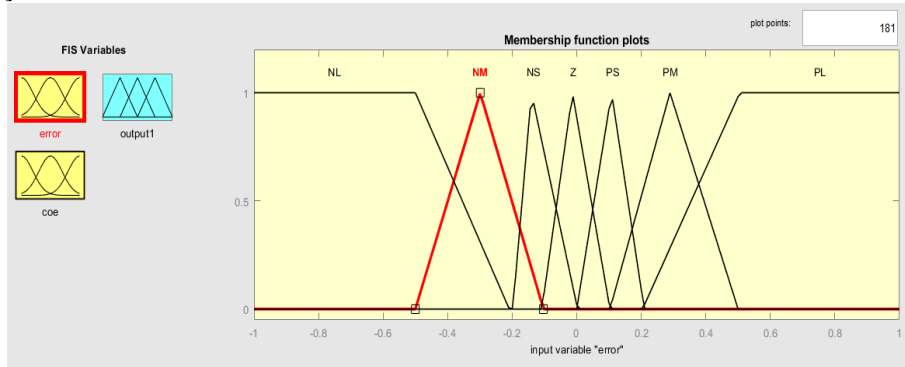


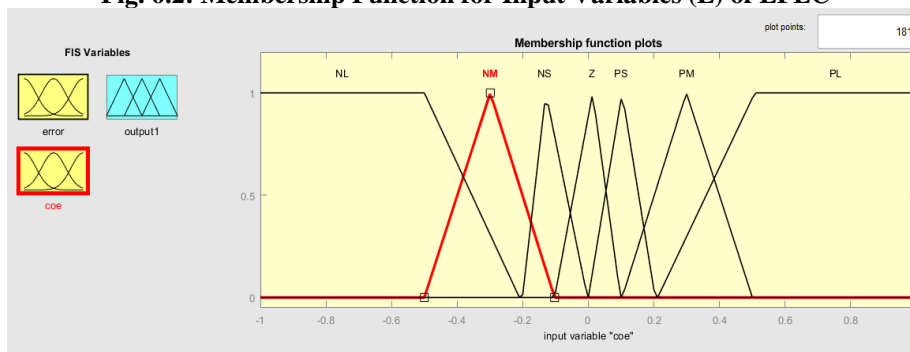**Fig. 6.2: Membership Function for Input Variables (E) of LFLC**



**Fig. 6.3: Membership Function for Input Variables (COE) of LFLC**
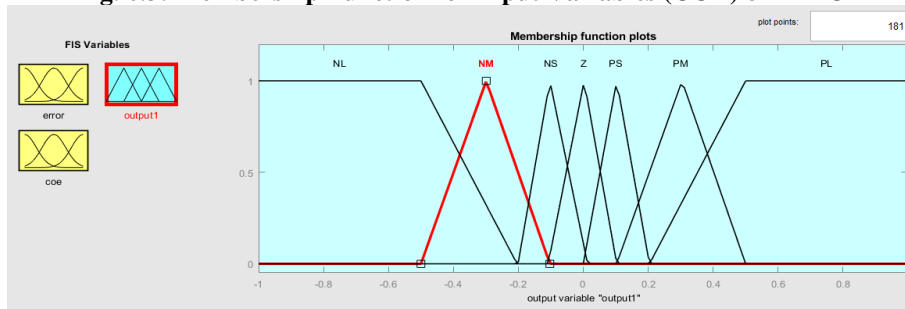


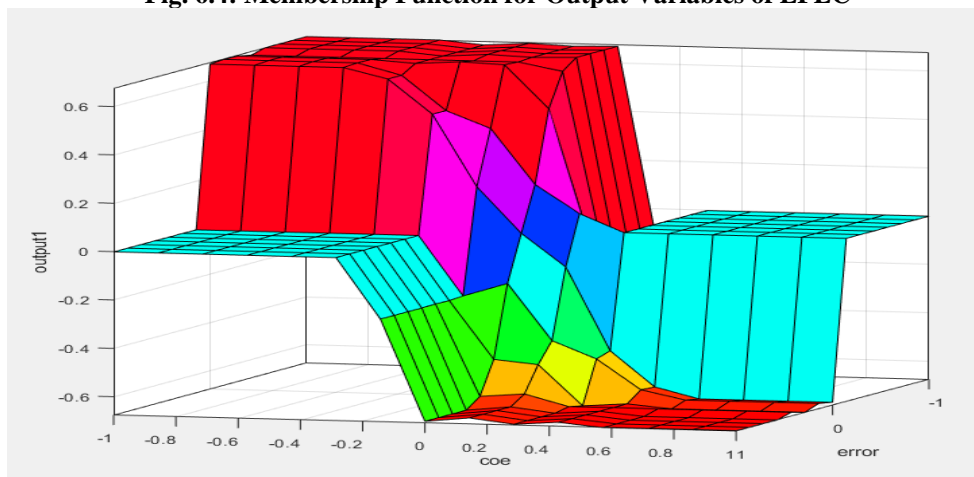**Fig. 6.4: Membership Function for Output Variables of LFLC**



**Fig. 6.5: Three-Dimensional Plot of the Control Surface**

As shown in Table 6.1, the fuzzy system rule base is created. It depicts the fuzzy controller's set of rules. The error variation E, change in error variation dE and output variation, i.e., duty cycle variation α, are all fuzzy input variables. The IF/THEN syntax is always used to express fuzzy rules. Here for switching loss, we use 49 rules like:

**Table-6.1 Fuzzy Rule Table for Output**

| dE \ E | NM | NS | ZE | PS | PM | NL | PL |
|---|---|---|---|---|---|---|---|
| NM | PL | PM | PM | ZE | ZE | PL | ZE |
| NS | PL | PS | PS | NM | NS | PL | NM |
| ZE | PM | PS | ZE | NS | NM | PL | NL |
| PS | PS | PS | NS | NS | NL | NM | NL |
| PM | ZE | ZE | NM | NM | NL | ZE | NL |
| NL | PL | PL | PL | ZE | ZE | PL | ZE |
| PL | ZE | ZE | NL | NL | NL | ZE | NL |

## 7. SIMULATION RESULTS AND DISCUSSION

This system presents, following different Simulink studies designed to investigate applications of proposed control strategy with power management model for hybrid generation system in stand-alone power generation mode.

**Case -1: Simulation Response at Impulse Change in Wind Speed, Successive Increase in Irradiance Level and Impulse Change in Load**

This case presents the scenario of impulse change in wind speed in stepped manner from 12 m/s to 8 m/s and further to 10 m/s and successive increase in irradiance level in stepped manner from 600W/m² to 800W/m² and further to 1000W/m² at varying load from 6.6 kW to 16 kW and further to 7.1 kW. The simulation results are shown below. Fig. 4.29 shows the simulation results of the PV system with the effect of successive increase in irradiance level. Fig. 7.1 shows the Irradiance (W/m²), PV Temperature ($^0$C), PV voltage (volt) and PV output power (kW). Fig. 4.29 clearly shows that at 600W/m² the power output is 5.9 kW. At t=1 sec when irradiance increased from 600W/m² to 800W/m² the power output also increased to 8 kW. At t=3 sec when irradiance increased from 800W/m² to 1000W/m², the power output further increased to 9.1 kW.
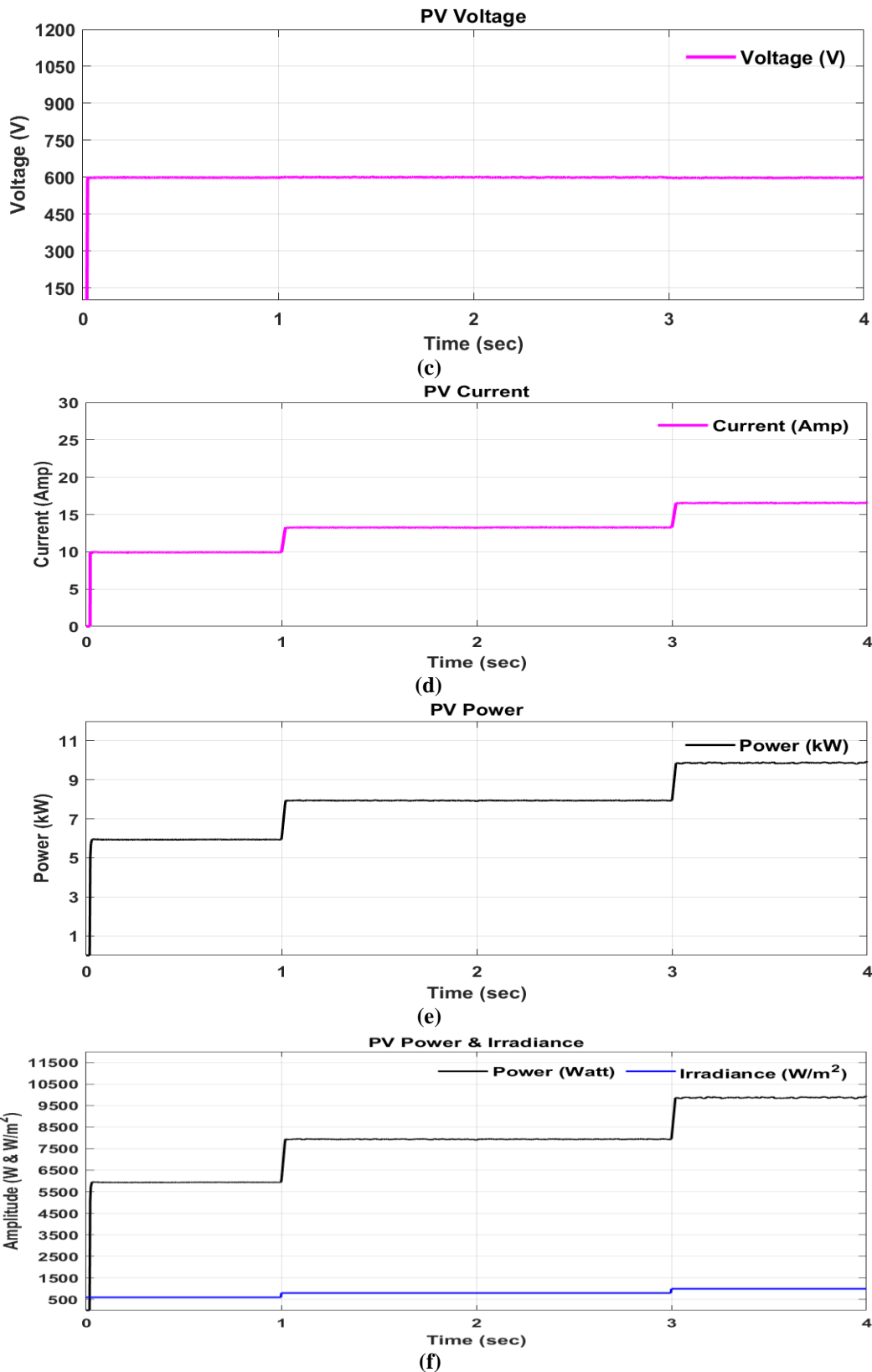


(a)



(b)

**(c)**



**(d)**



**(e)**



**(f)**
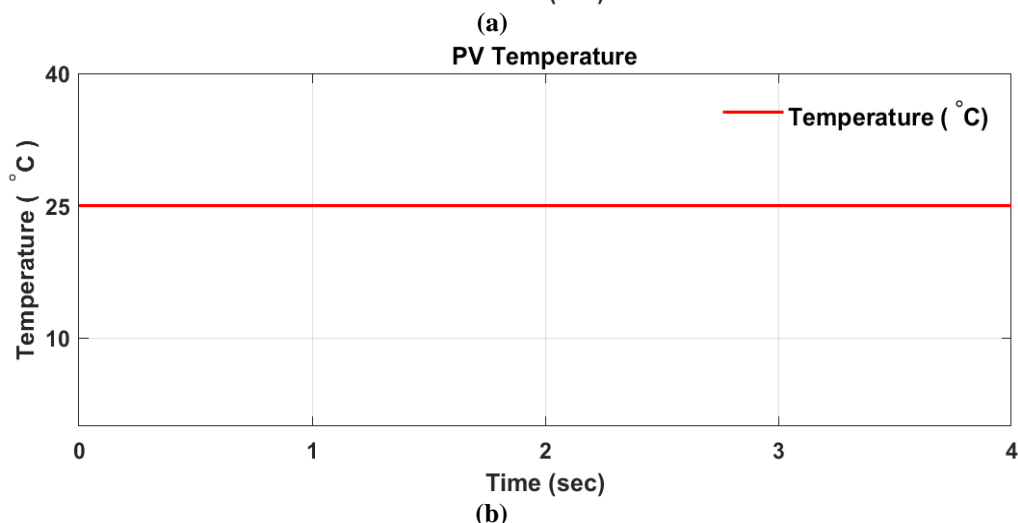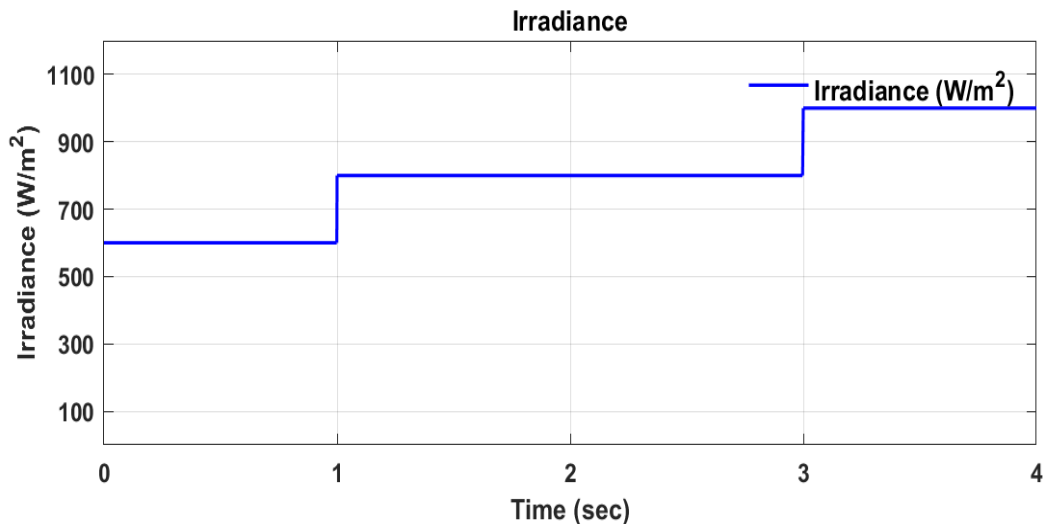
**Fig. 7.1 Simulation results of PV system with irradiance change from 600 W/m² to 800 W/m², 800 W/m² to 1000 W/m², (a) waveform of Irradiance (W/m2), (b) PV Temperature (°C), (c) PV Voltage (volt), (d) PV Current (Amp), (e) PV output power(kW) and, (f) PV output power(W) with irradiance**

Fig. 7.2 shows the simulation results of the PMSG based WECS with impulse change in wind speed from 12 m/s to 8 m/s and further to 10 m/s. Fig. 7.2 shows the input wind speed $\omega_s$, PMSG speed $\omega_m$, PMSG output power $P_{ac}$, electromagnetic & mechanical torque $T_e \& T_m$, PMSG phase to phase voltages $V_{ab,bc}, V_{ca}$, and PMSG phase current $I_a, I_b, I_c$. Fig. 7.2 clearly shows that at input wind speed 12 m/s and PMSG speed is 1415 rpm. the power output is 6300 Watt. At t=2 sec when input wind speed decreased from 12 m/s to 8 m/s and PMSG speed is decreased at 950 rpm, the power output also decreased to 1930 Watt. At t=4 sec when input wind speed increased from 8 m/s to 10 m/s and PMSG speed is increased at 1200 rpm, the power output also increased to 3750 Watt.

International Journal of Technical Research & Science



**PMSG Input Wind Speed $\omega_s$**

(a)

**PMSG Rotor Speed $\omega_m$**

(b)

**PMSG Output Power $P_{ac}$**

(c)

**PMSG Electromagnetic & Mechanical Torque $T_e$ & $T_m$**

(d)

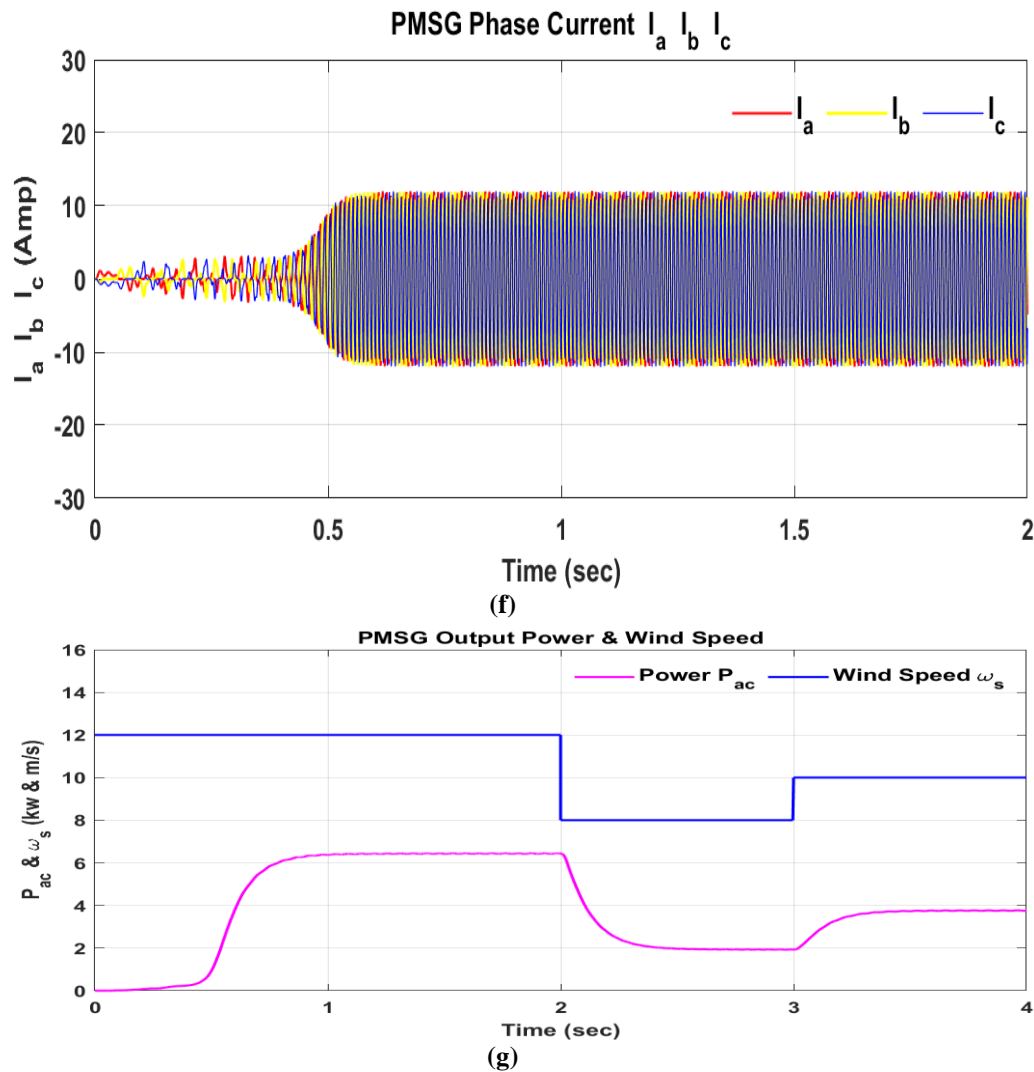**PMSG Phase to Phase Voltages**

(e)

**pg. 8**

**(f)**



**(g)**
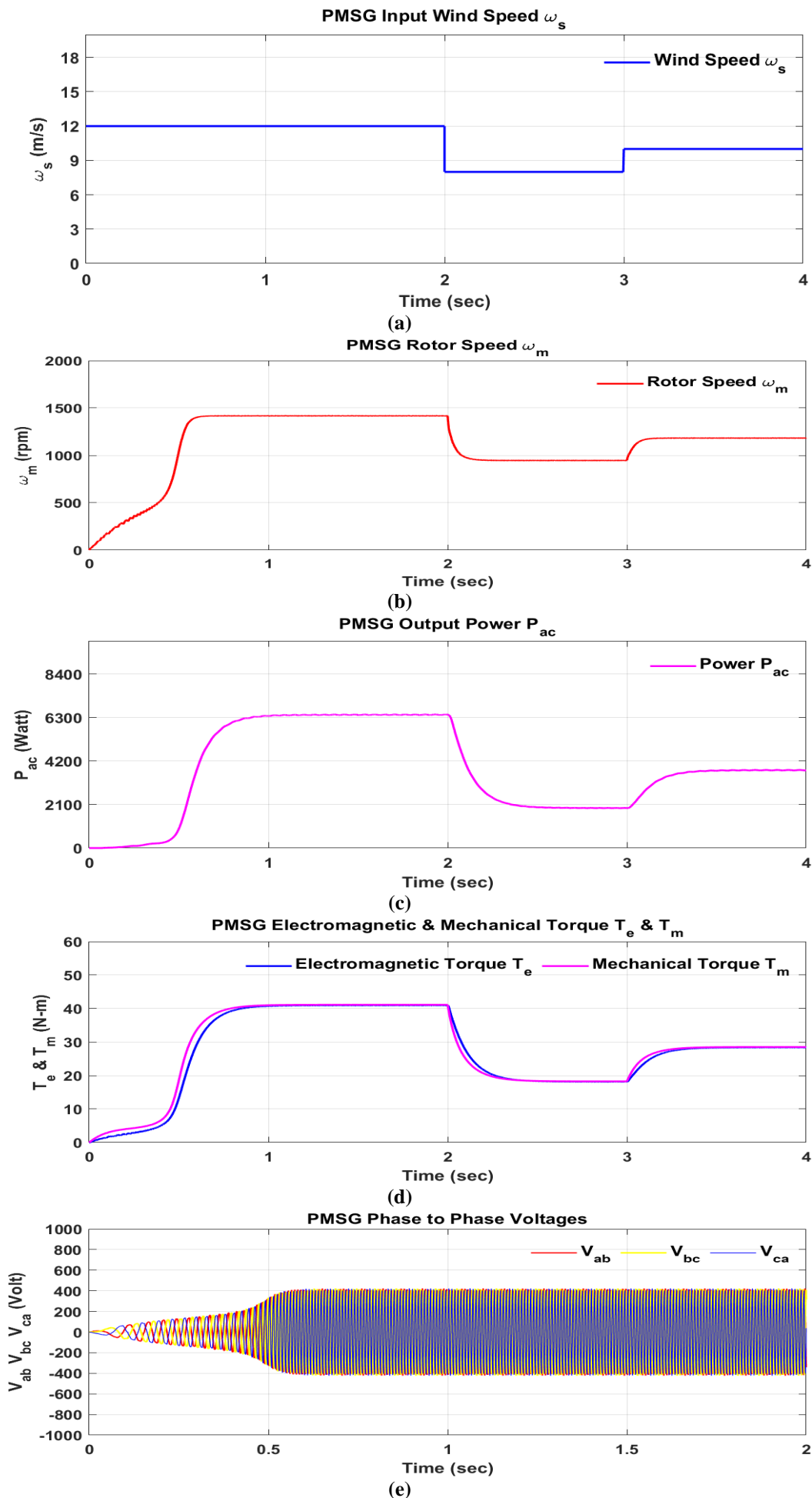
**Fig. 7.2 Simulation results for PMSG based WECS for input wind speed change from 12 m/s to 8 m/s, 8 m/s to 10 m/s Waveform of, (a) input wind speed $\omega s$, (b) PMSG speed $\omega m$, (c) PMSG output power $Pac$, (d) Electromagnetic & mechanical torque $Te \& Tm$, (e) PMSG phase to phase voltages $VabVbcVca$, (f) PMSG phase current $IaIbIc$ and, (g) PMSG output power with wind speed**

The output from the PV system and WECS are fed to the common DC link bus. A power management strategy is developed, to manage the generated power. A battery storage system integrated at the same DC link bus with an intermediate DC-DC Buck-Boost converter. In the control algorithm, FLC is used to manage the power of the hybrid system with the battery storage system.

Fig. 7.3 shows the simulation results of the battery storage system. It shows the battery voltage, battery current and battery SOC (State of change). Fig. 7.3 (a) clearly shows result that the voltage of the battery remains constant at 340V. The initial SOC of the battery is set at 60% during the simulation. As the load demand is not higher than the generated power so the extra generated power fed to the battery through a DC-DC converter. As seen from the battery current waveform in Fig 7.2 (b) initially at time t=0.5 sec PV system working at 600W/m² and WECS at 12m/s the current fed to the battery is about 18A.

As the battery is getting current from the hybrid system so it started charging and SOC is started increasing. At time t=1 sec power output from the PV system increase as irradiance level changed from 600W/m² to 800 W/m² and WECS at 12m/s. As a result of this current fed to the battery is also increased from 18A to 22A and the rate of rising of SOC also increased shown in Fig. 7.1 (c). Further, at time t=2 sec power output from the PV system irradiance 800 W/m² and power output from the WECS system decrease as input wind speed changed from 12 m/s to 8 m/s. As a result of this, current fed to the battery is also decreased from 20A to 10A and the rate of rising of SOC also increased. Further, at time t=3 sec power output from the PV system increase as irradiance changed from 800W/m² to 1000 W/m² and power output from the WECS as input wind speed 8 m/s. As a result of this, current fed to the battery is also increased from 10A to 16A and the rate of rising of SOC also increased. Further, at time t=4 sec power output from the PV system as irradiance 1000 W/m² and power output from the WECS system increase as input wind speed changed from 8 m/s to 10 m/s. As a result of this, current fed to the battery is also increased from 16A to 21A and the rate of rising of SOC further increase.
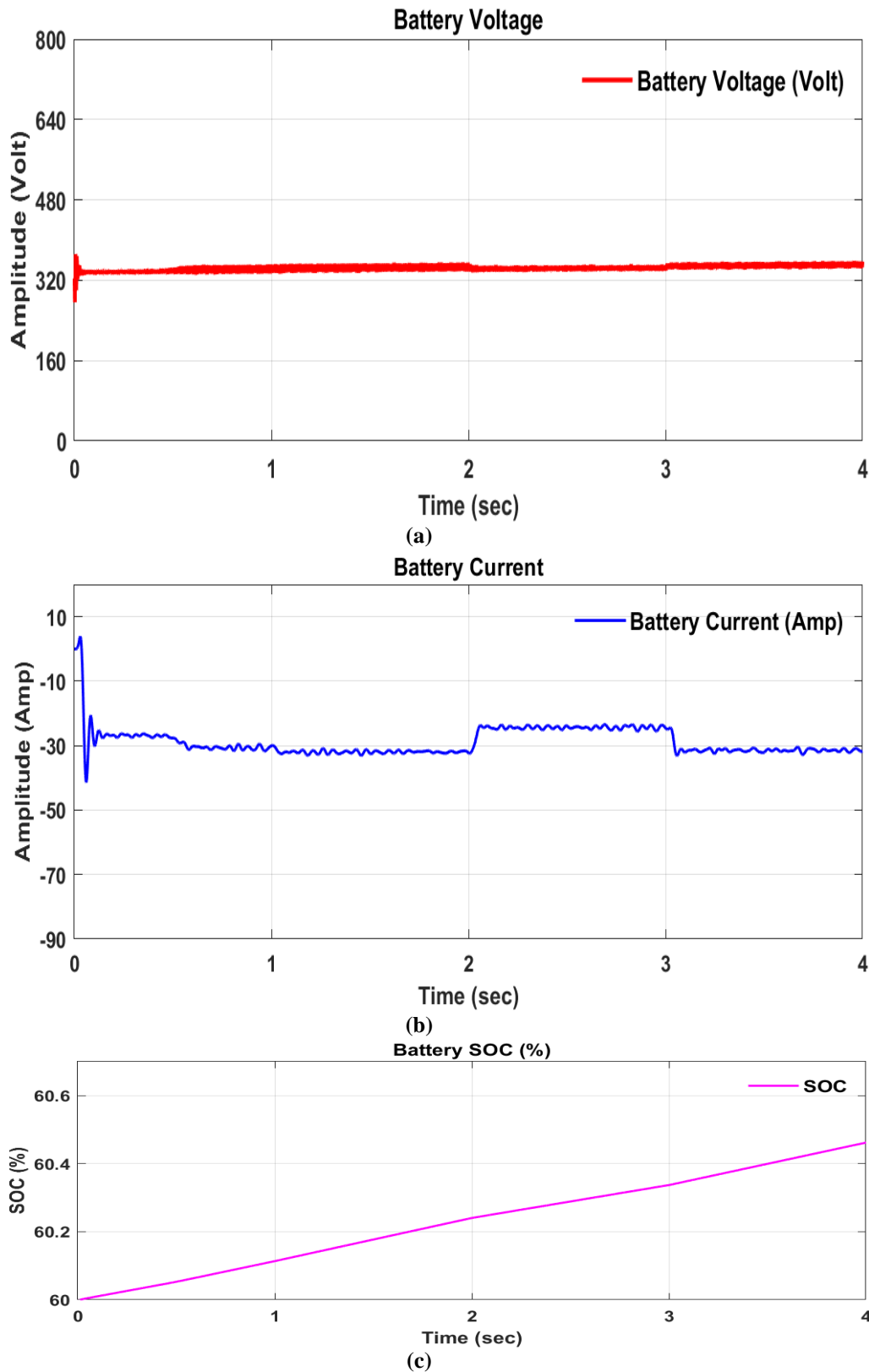
**Fig. 7.3 Simulation Results for Battery system, Waveform of (a) Battery Output Voltage (volt),**
**(b) Battery Output Current (Amp), (c) Battery SOC (%)**

Fig. 7.4 (b) shows the simulation result of DC bus reference voltage and actual DC bus voltage, switching pulses switch $S_1$ and $S_2$ of DC-DC buck-boost converter and controller output. Fig. 7.4 (b) shows that the control strategy is able to maintain constant DC bus voltage.

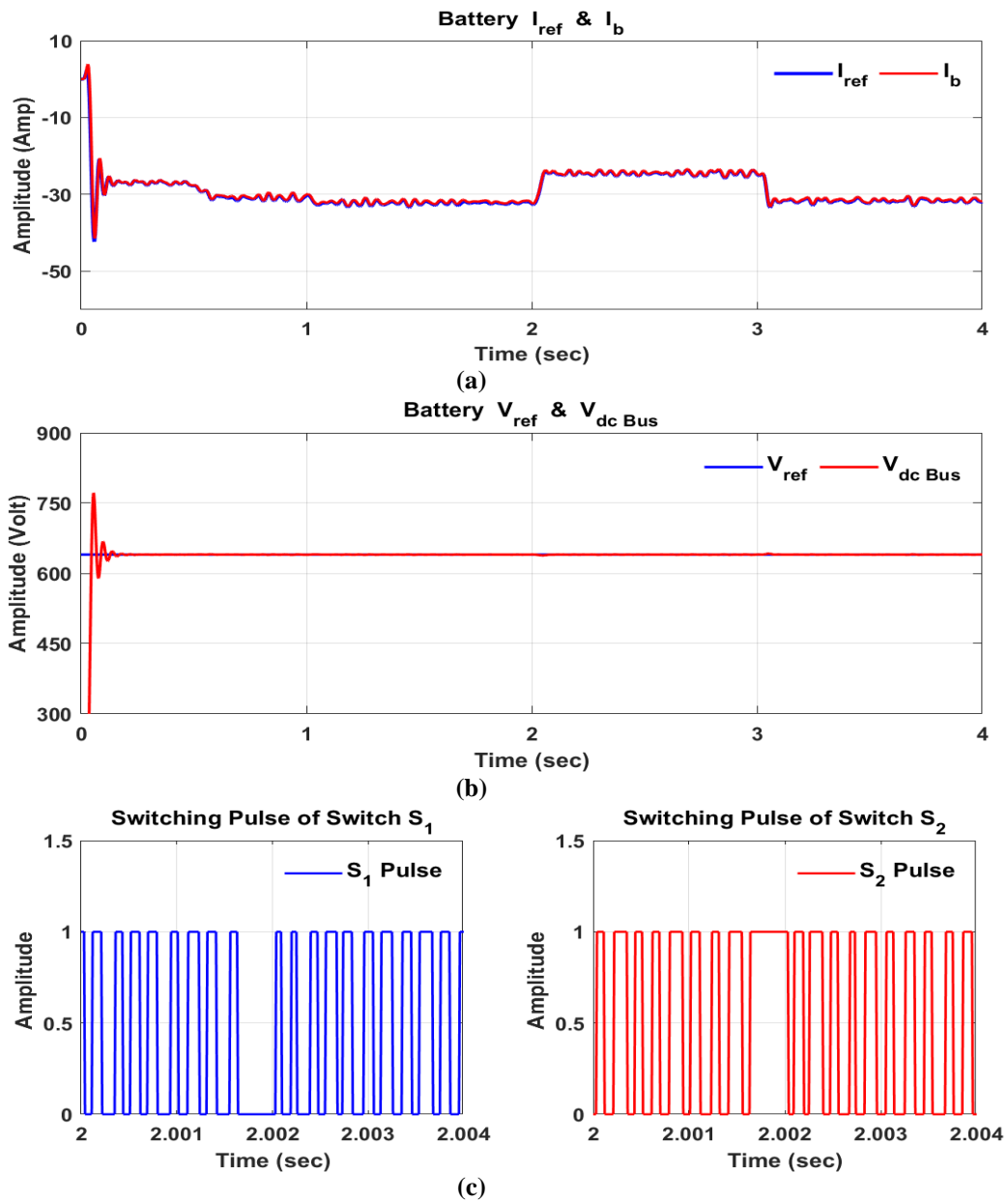International Journal of Technical Research & Science



**Fig. 7.4 Simulation Results for Power Management system, Waveform of (a) Battery current with reference current, (b) Reference voltage with dc bus voltage and, (c) Switching pulses of switch $S_1$ & $S_2$**

Now, this generated DC bus voltage fed to the multilevel inverter. The fuzzy logic controller controlled inverter AC output voltage fed to the load. Fig. 7.6 shows the multilevel inverter output voltage of the inverter. Switching pulses of the inverter are shown in Fig. 7.6.
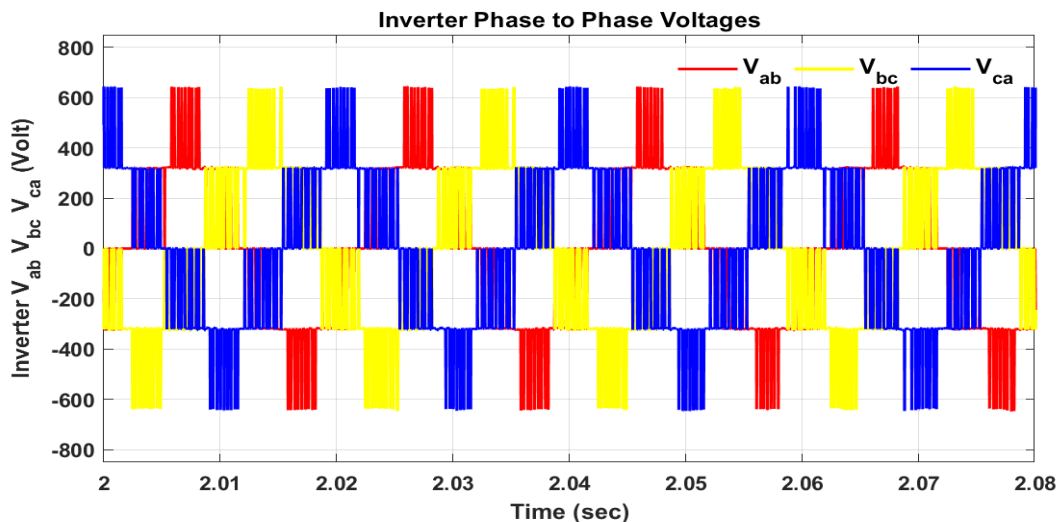


**Fig. 7.5 Multilevel Inverter output phase to phase voltages $V_{ab}, _{bc}, V_{ca}$**
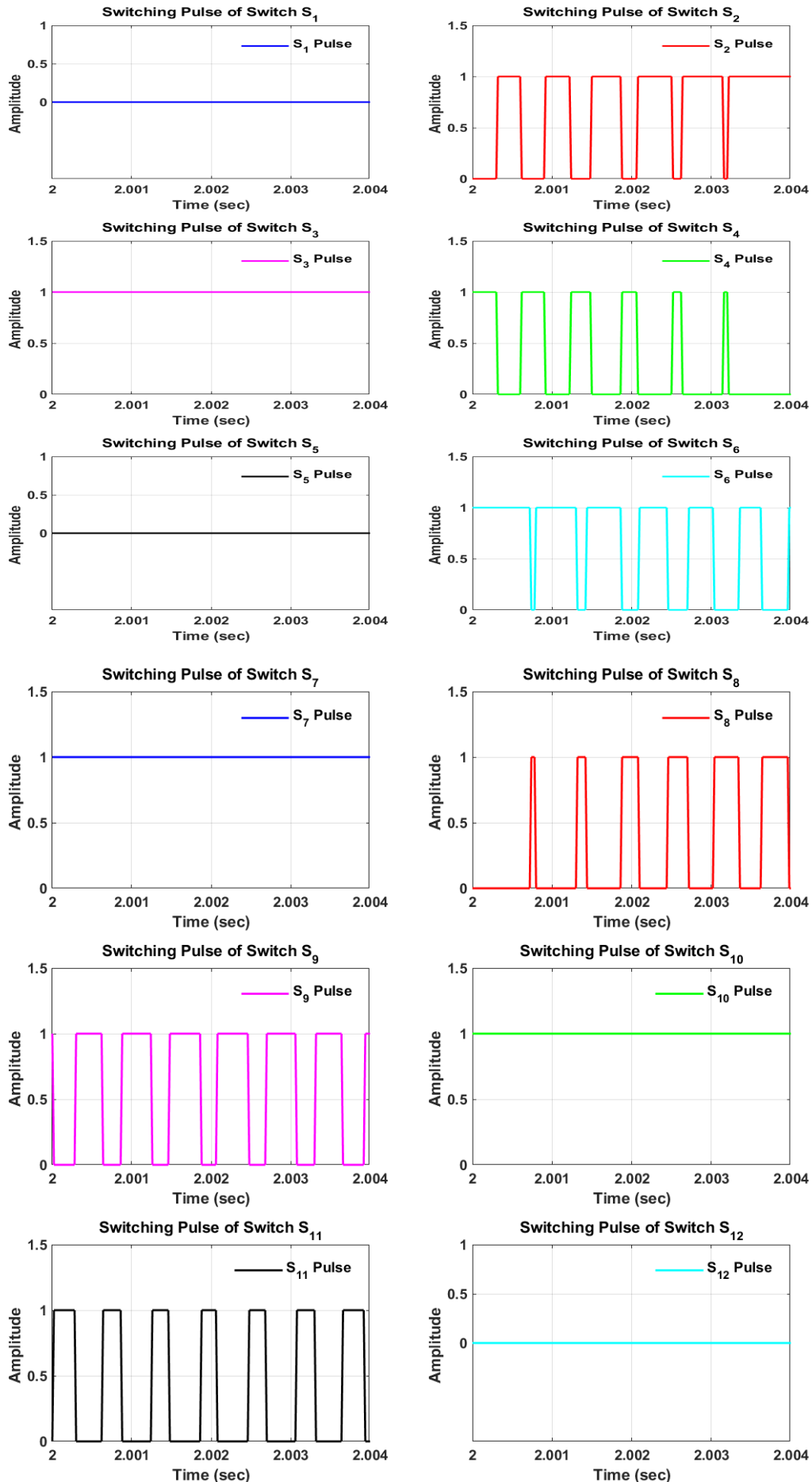
International Journal of Technical Research & Science



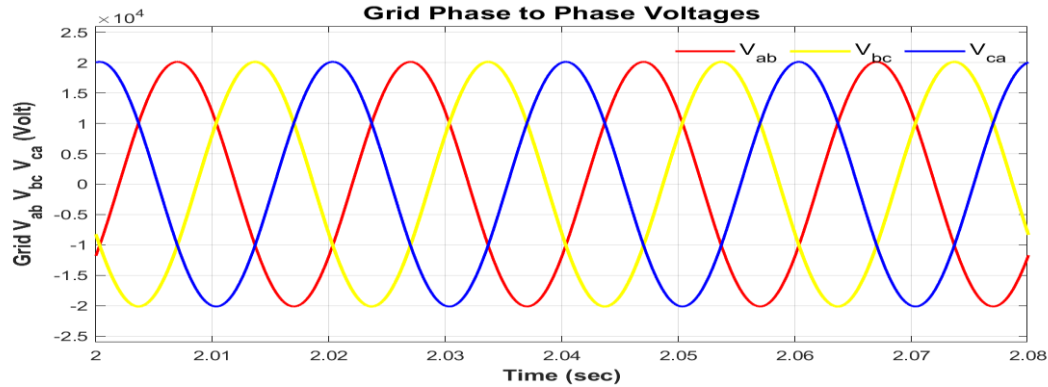**Fig. 7.6 Switching pulses waveform of inverter switches**

**Fig. 7.7 Simulation Results for Grid, Waveform of Phase-Phase Voltage**

In this case, the comparison of load demand, battery system, WECS, and PV system power is shown in Fig. 7.8. As in this case the load is varying. Also, during impulse change in wind speed in stepped manner, so the power output of the WECS system is varying correspondingly. Also, during successive increase in irradiance level in stepped manner, the power output of the PV system is varying correspondingly. As seen from the result that during the time interval, 0 to 1-sec load remain unchanged PV system output is also constant. The generation from the PV system is enough to meet the load demand. As WECS is not in steady-state operation so power generation initially is very low, after a time delay of about 0.5-sec WECS power output increases. So now total generated power from the PV system and WECS is more than the demanded load situation so as from time interval 0.5 sec extra generated power fed to the battery system to store energy. Fig 4.46 shows the result that when at time interval 1 to 1.5-sec load remain constant power output of the PV system is increased and WECS output is also constant than power fed to the battery is also increased. Further, At time interval 1.5 to 2-sec load suddenly change the power output of the PV system and WECS remain unchanged than power fed to the battery is also decreased. So now total generated power from the PV system and WECS is less than the demanded load situation so as from time interval 1.5-sec extra power consumption through the battery system.
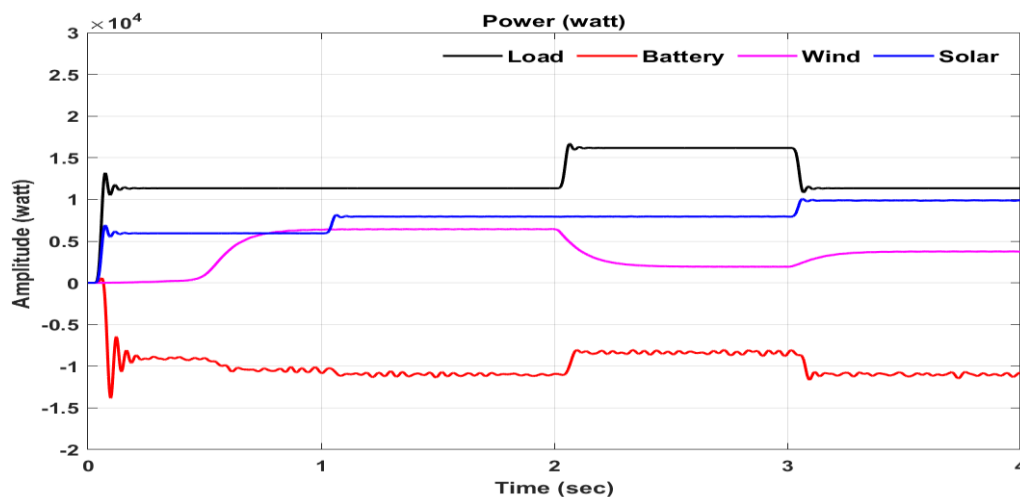


**Fig. 7.8 Power levels of load, battery, wind and solar system**

Further, at time interval 2 to 2.5-sec load remain constant power output of the PV system remains unchanged and WECS suddenly changed than power fed to the battery is also decreased. So now total generated power from the PV system and WECS is less than the demanded load situation so as from time interval 2 to 2.5-sec extra power consumption through the battery system. Further, at time interval 2.5 to 3-sec load suddenly changed the power output of the PV system & WECS remain unchanged than power fed to the battery is also increased. So now total generated power from the PV system and WECS is more than the demanded load situation so as from time interval 2.5 to 3 sec extra generated power fed to the battery system to store energy. Further, at time interval 3 to 3.5-sec load remain constant power output of the PV system suddenly increase and WECS remain unchanged than power fed to the battery is also increased. So now total generated power from the PV system and WECS is more than the demanded load situation so as from time interval 3 to 3.5 sec extra generated power fed to the battery system to store energy. Further, at time interval 3.5 to 4-sec load suddenly change, the power output of the PV system and WECS remain unchanged than power fed to the battery is also decreased. So now total generated power from the PV system and WECS is less than the demanded load situation so as from time interval 3.5 to 4-sec extra power consumption through the battery system. Further, at time interval 4 to 5-sec load remain constant power output of the PV system remains unchanged and WECS suddenly changed than power fed to the battery is also increased. So now total generated power from the PV system and WECS is more than the demanded load situation so as from time interval 4 to 5 sec extra generated power fed to the battery system to store energy.

International Journal of Technical Research & Science

## CONCLUSION

In this paper, an OT controller is implemented for Alone HRES power control. It works according to the system's strategies to control flow of power. The performance of the controller is good under different situations of power generation and consumption of the same by loads. It maintains the SOC of battery within limits i.e. to say between specified maximum and minimum limits. As proposed, it keeps the SOC above 80% all the time. The propose system has been designed and modeled using MATLAB/Simulink. With results it is verified that the control unit (OT and PMU) designed keeps the balance between power supply and the load demanded irrespective of sudden change of loads and power generation.

## REFERENCES

[1] Nema, P; Nema, R.K and Rangnekar, S. "A Current and Future state of art development of Hybrid Energy system using Wind and PV Solar," Elsevier Renewable and Sustainable Reviews, Vol. 13, October 2009, pp.2096-2103.

[2] Sassi, A., Zaidi, N., Nasri, O and Slama, J.B.H. 2017. Energy management of PV/wind/battery hybrid energy system based on batteries utilization optimization, IEEE International Conference on Green Energy Conversion Systems held at Tunisia during Mar. 23-25, 2017, pp. 1-7.

[3] Rehman, S; Alam, MD.M; Meyer, J.P and Al-Hadhrami, L.M. " Feasibility study of a wind-pv-diesel hybrid power system for a village," Elsevier Renewable Energy, vol. 38, Febuary 2012, pp.258- 268.

[4] Khan, B.H "Non-Conventional Energy Resources," Tata McGraw-Hill Pub.Co., 2009.

[5] Dali, M., Belhadj, J., Roboam, X.: 'Hybrid solar-wind system with battery storage operating in grid–connected and standalone mode: Control and energy management-experimental investigation', Energy, 2010, 35, pp. 2587–2595.

[6] Nguyen, X. H. and Nguyen, M. P. 2015. Mathematical modeling of photovoltaic cell/module/arrays with tags in Matlab/Simulink, Environmental Systems Research.4(1):1-13.

[7] Kamal, T., Karabacak, M., Hassan, S. Z., Li, H., Arsalan, A., & Rajkumar, R. K. 2017. Integration and control of an off-grid hybrid wind/PV generation system for rural applications. International Conference on Innovations in Electrical Engineering and Computational Technologies held at Karachi, during 5-7 April 2017, pp. 1-6.

[8] Priyadarshi, N., Padmanaban, S., Ionel, D. M., Popa, L. M. and Azam, F., "Hybrid PV-Wind, micro-grid development using quasi-z-source inverter modeling and control-experimental investigation," Energies, vol. 11, pp.1-15, 2018.

[9] Zeng, J., Ning, J., Du, X., Kim, T., Yang, Z. and Winstead, V., "A four-port DC-DC converter for a standalone wind and solar energy system," IEEE Transactions on Industry Applications, vol. 56, pp. 446-454, 2020.

[10] Khateb, A. H. E., Rahim, N. A., Selvaraj, J. and Williams, B. W., "DC-to-DC converter with low input current ripple for maximum photovoltaic power extraction," IEEE Transactions on Industrial Electronics, vol. 62, pp. 2246-2256, 2015.

[11] Ahmadi, M. and Shenai, K., "New, efficient, low-stress buck/boost bidirectional DC-DC converter," In: Proceedings of IEEE Energy tech conference held at Cleveland during May 29-31, 2012, pp. 1-6.

[12] Wandhare, R.G. and Agarwal, V., "Novel integration of PV-Wind energy system with enhanced efficiency," IEEE Transactions on Power Electronics, vol. 30, pp. 3638-3649, 2015.

[13] Sharma, A. and Jamuna, K., "Coordination of energy storage devices in hybrid power systems," In: Proceedings of Springer International conference on Emerging Trends in Electrical, Communications and Information Technologiesheld at India during November 15-16, 2016, pp. 327-336.

[14] Manandhar, U., Tummuru, N. R. and Kollimalla, S. K., "Validation of faster joint control strategy for battery- and super capacitor-based energy storage system," IEEE Transactions on Industrial Electronics, vol. 65, pp. 3286-3295, 2018.

[15] Lei, M., Yang, Z., Wang, Y., and Honghua, X., "Design of energy storage control strategy to improve the PV system power quality," In: Proceedings of IEEE 42$^{nd}$ Annual Conference of the Industrial Electronics Society (IECON) held at Italy during October 23-26, 2016, pp. 2022-2027.

[16] Faria, J., Pombo, J., Calado, M. and Mariano, S., "Power management control strategy based on artificial neural networks for standalone PV applications with a hybrid energy storage system," Energies, vol. 12, no.2, pp. 1-24, 2019.